OXFORD

Journal of Geophysics and Engineering

Journal of Geophysics and Engineering (2020) **17**, 277–299 doi:10.1093/jge/gxz105

On the applicability of a renormalized Born series for seismic wavefield modelling in strongly scattering media

Xingguo Huang [1,2,*], **Morten Jakobsen**[1] **and Ru-Shan Wu**[2]

[1] University of Bergen, Department of Earth Science, Allegaten 41, 5020 Bergen, Norway
[2] University of California, Earth and Planetary Sciences, Modeling and Imaging Laboratory, 1156 High Street, Santa Cruz, CA 95064, USA

*Corresponding author: Xingguo Huang. E-mail: xingguo.huang@uib.no, xingguo.huang19@gmail.com

Received 25 April 2019, revised 4 November 2019
Accepted for publication 15 November 2019

Abstract

Scattering theory is the basis for various seismic modeling and inversion methods. Conventionally, the Born series suffers from an assumption of a weak scattering and may face a convergence problem. We present an application of a modified Born series, referred to as the convergent Born series (CBS), to frequency-domain seismic wave modeling. The renormalization interpretation of the CBS from the renormalization group prospective is described. Further, we present comparisons of frequency-domain wavefields using the reference full integral equation method with that using the convergent Born series, proving that both of the convergent Born series can converge absolutely in strongly scattering media. Another attractive feature is that the Fast Fourier Transform is employed for efficient implementations of matrix–vector multiplication, which is practical for large-scale seismic problems. By comparing it with the full integral equation method, we have verified that the CBS can provide reliable and accurate results in strongly scattering media.

Keywords: seismic modeling, integral equation, wave scattering, renormalization theory

1. Introduction

The integral equation (IE) method based scattering theory (Aki & Richards 1980; Zhdanov 2002) is a powerful tool in the modeling of wave propagation, which has a wide application in data processing (Weglein *et al.* 1997, 2003), modeling (Innanen 2009), and seismic inversion (Wu & Zheng 2014; Snieder 1990; Berkhout 2012; Zhang & Weglein 2009; Alkhalifah & Wu 2016; Alkhalifah 2016; Wu & Alkhalifah 2017; Huang *et al.* 2019). An attractive features of the IE method is that only the anomalous volume (scattering volume) needs to be discretized, which leads to more efficient computation (Malovichko *et al.* 2017). The implementation of the IE method involves dividing the medium into background and anomalous parts (Zuberi & Alkhalifah 2014).

The Born series has an assumption of weak scattering (Wu & Toksoz 1987; Kouri & Vijay 2003). Convergence issues may occur in strongly scattering areas, such as salt structures. It is important for seismic imaging in such strong-contrast regions to address the weak-scattering assumption. One important approach that addresses the divergence problem is to renormalize the Born series using various renormalization approaches (Eftekhar *et al.* 2018).

There are several approaches to develop a convergent scattering series. There have been successful attempts to introduce the De Wolf approximation (De Wolf 1971, 1985) into seismic scattering series (Wu & Huang 1995). The renormalized scattering series is derived by Jakobsen & Wu (2016) using the T-matrix and De Wolf series. The T-matrix is a

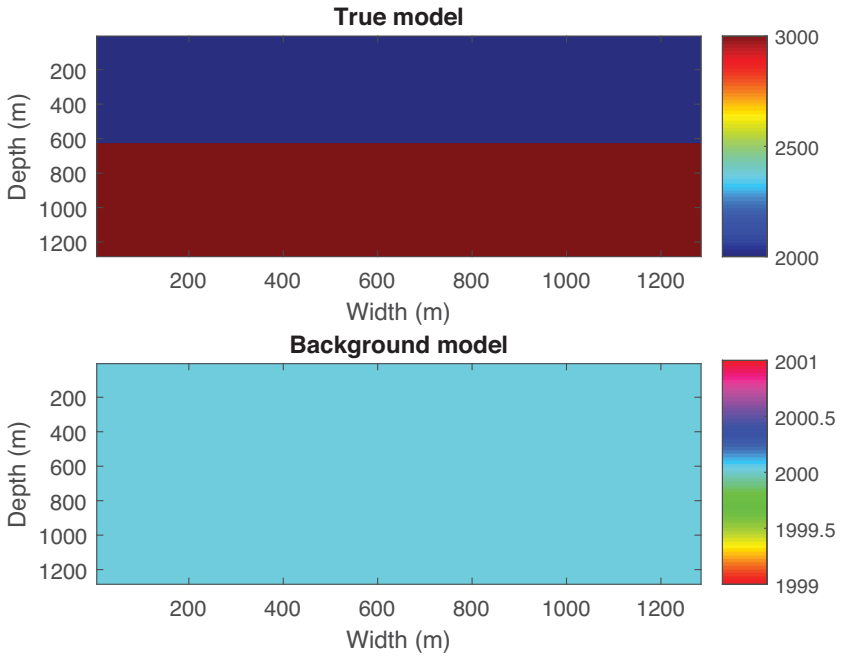

Figure 1. The two-layered and background models. The size of the model is 1280 m × 1280 m.

transition operator that includes all the effects of multiple scattering. Renormalization group method has been applied to seismic waveform inversion (Wu *et al.* 2015) and envelope inversion (Wu *et al.* 2016). Signicant progress has been made by Yao *et al.* (2015) by dividing the renormalized Lippmann–Schwinger equation into two sub-Volterra type integral equations and introducing wavefield separation. Recently, by employing the renormalization group (RG) theory, we developed a renormalized version of the Born series. Numerical tests showed that this solution can be convergent for large-contrast media (Jakobsen *et al.* 2018). Our renormalization group approach is based on the use of an auxillary set of scale-dependent scattering potentials, which gradually evolves toward the real physical scattering potential.

Another interesting convergent Born series (CBS) was proposed by Osnabrugge *et al.* (2016) to solve the Helmholtz equation. The convergent Born series can guarantee convergence by localizing the wavefields, in which the contracted preconditioner must be specified. Actually, the CBS can be understood as a kind of renormalized Born series based on the RG theory. In the early 1970s, the renormalization procedure was proposed by Gell-Mann & Low (1954) for problems of infinity and divergence. From the early 1970s (Wilson 1971), RG theory has been widely used to remove divergence in quantum physics, critical phenomena, dynamical systems and statistical mechanics, etc. The major purpose of the RG theory is to obtain stable properties of physical systems (Goldenfeld 1992). Based on the above fact, Chen *et al.* (1994, 1996) applied the RG approach to deriving global asymptotic solutions of differential equations. Since then, the RG theory has been well developed and significant progress in renormalizing perturbation series (Yakhot & Orszag 1986; Pelissetto & Vicari 2002; Delamotte 2004; Kirkinis 2008, 2012) has been made.

The purpose of this paper is to extend the CBS of Osnabrugge *et al.* (2016) to seismic scattering problems for strongly scattering media and compare the CBS with the full integral equation method. The convergent Born series is obtained by localizing the Green's function with a dampling factor. From the technical point of view, the CBS removes the divergence by localizing the wavefields and controlling convergence using a preconditioner. Thus, the CBS can be understood as a kind of renormalized Born series. After presenting the convergent Born series, we analyze the theoretical background of the convergent Born series from the renormalization group theory prospective and its nature of localization. Then, we give numerical results of frequency-domain wavefields. To quantatively compare the results from the CBS and full integral equation methods, we present numerical results for results of pressure wavefields in strongly scattering media.

2. Integral equations for the seismic scattering problem

2.1. *The Lippmann–Schwinger equation*

The Helmholtz equation can be written as (Morse & Feshback 1953):

$$\nabla^2\psi(\mathbf{r}) + k^2\psi(\mathbf{r}) = -s(\mathbf{r}), \tag{1}$$

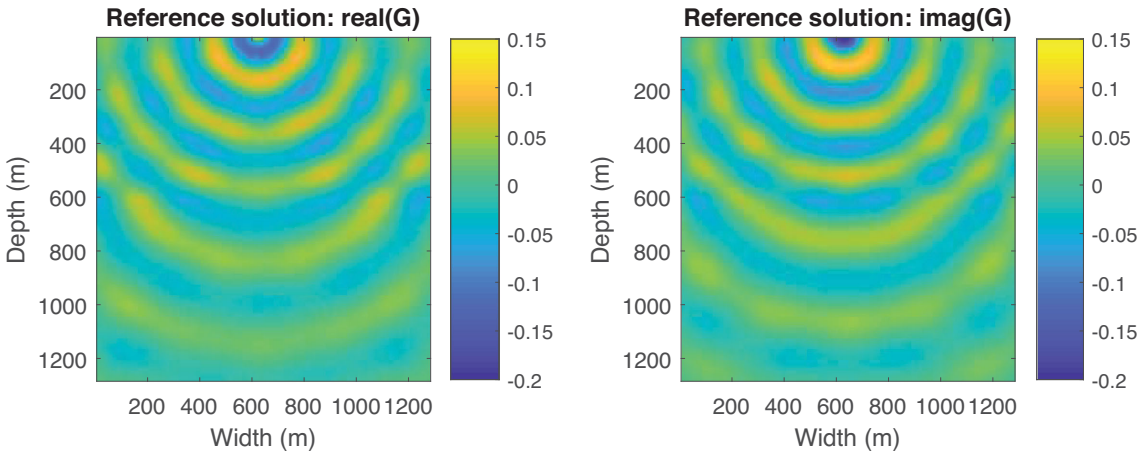

(a)

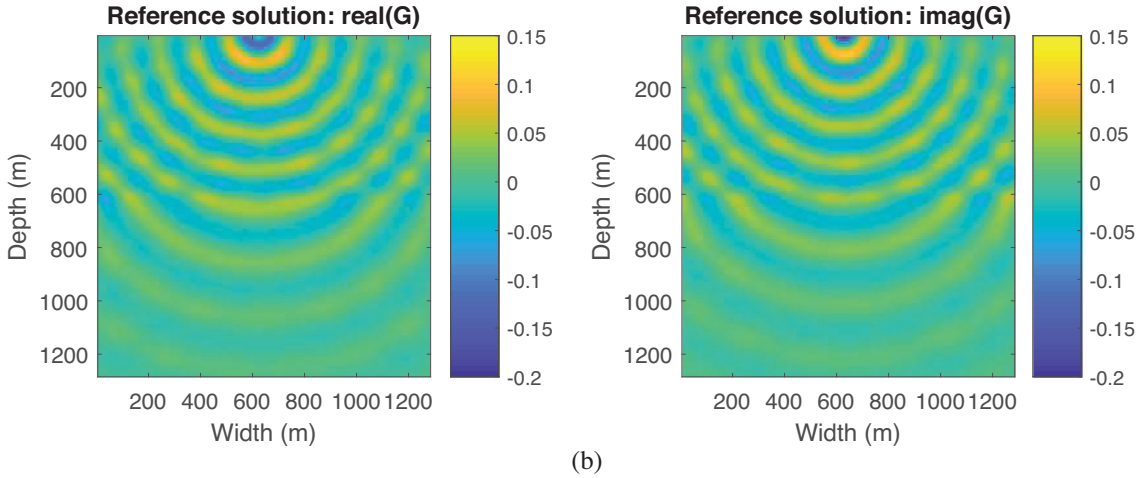

(b)

Figure 2. Frequency-domain wavefields for the frequency of (a) 10 Hz and (b) 15 Hz for the two-layer model using the IE method.

with the wavenumber k and source signal $s(\mathbf{r})$, where ∇ is the second-order differentiation. Defining $\psi_b(\mathbf{r})$ as the background field,

$$\nabla^2\psi_b(\mathbf{r}) + k_b^2\psi_b(\mathbf{r}) = -s(\mathbf{r}), \tag{2}$$

where k_b is the background wavenumber. The total wavefield $\psi(\mathbf{r})$ can expressed as

$$\psi(\mathbf{r}) = \psi_b(\mathbf{r}) + \psi_s(\mathbf{r}), \tag{3}$$

where k_s is the scattered wavenumber and $k_s = k - k_b$. Substituting equation (3) into (1), we have the following equation for the scattered wavefields $\psi_s(\mathbf{r})$:

$$-\nabla^2\psi_s(\mathbf{r}) - k_b^2\psi_s(\mathbf{r}) = k_s^2(\mathbf{r})\left(\psi_b(\mathbf{r}) + \psi_s(\mathbf{r})\right). \tag{4}$$

From equations (2) and (4), we get the scattered wavefields $\psi_s(\mathbf{r})$

$$\psi_s(\mathbf{r}) = k_b^2\int_D G_b(\mathbf{r},\mathbf{r}')\,\chi(\mathbf{r}')\,\psi(\mathbf{r}')\,d^3\mathbf{r}' \tag{5}$$

with

$$\chi(\mathbf{r}') = \frac{k^2 - k_b^2}{k_b^2}, \tag{6}$$

where the background Green's function G_b can also be calculated with analytical expressions for homogeneous media, and the ray theory (Cerveny 2005; Huang & Greenhalgh 2019), Gaussian beam (Huang *et al.* 2016a, b, 2018; Huang 2018) or finite difference method (Carcione 2007) for inhomogeneous media. Finally, we can get the Lippmann–Schwinger equation:

$$\psi(\mathbf{r}) = \psi_b(\mathbf{r}) + k_b^2\int_D G_b(\mathbf{r},\mathbf{r}')\,\chi(\mathbf{r}')\,\psi(\mathbf{r}')\,d^3\mathbf{r}'. \tag{7}$$

2.2. *The conventional Born series*

Equation (7) has the formal solution as

$$\psi(\mathbf{r},k) = \psi_b(\mathbf{r},k)\left(1 - k_b^2\int_D G_b(\mathbf{r},\mathbf{r}',k)\,\chi(\mathbf{r}')\,d^3\mathbf{r}'\right)^{-1}. \tag{8}$$

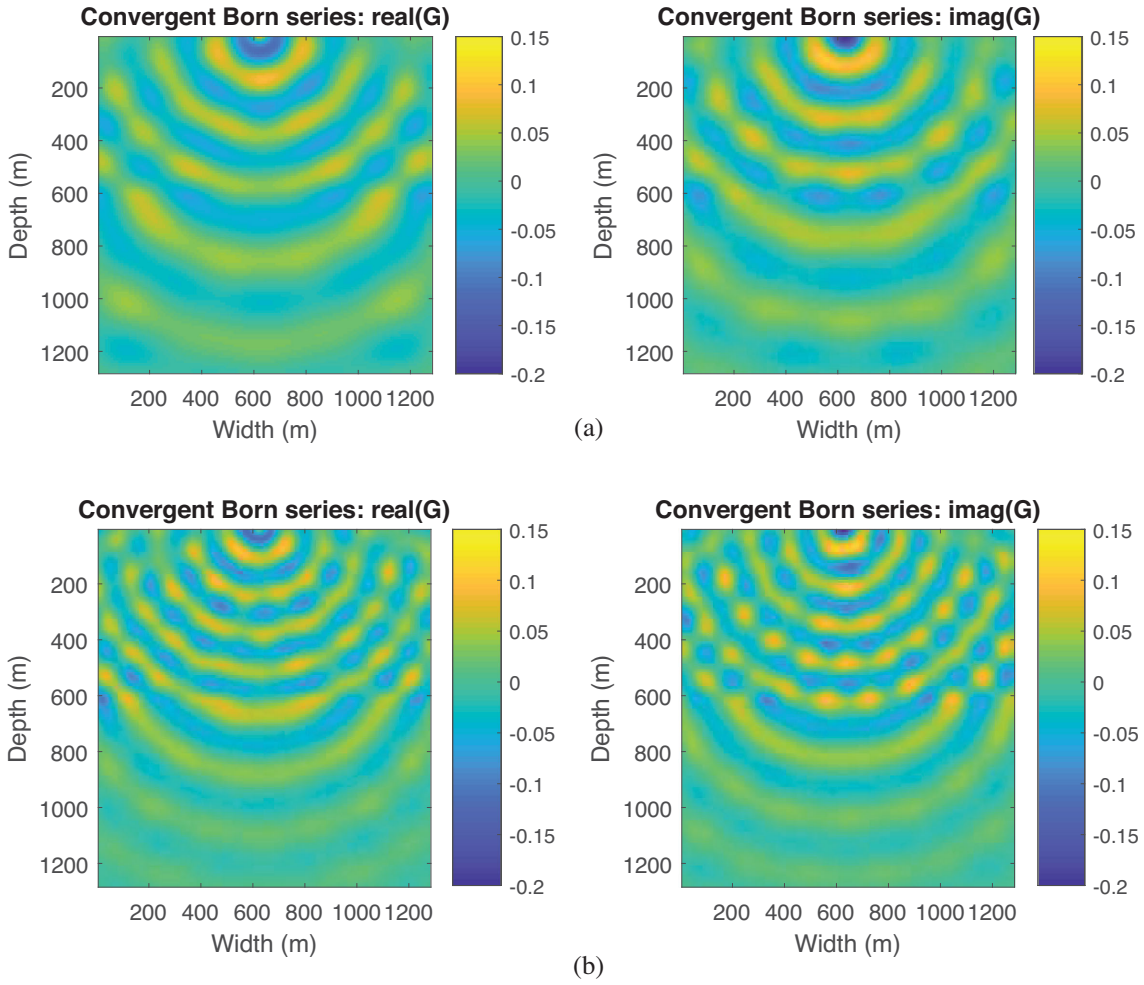

Figure 3. Frequency-domain wavefields for the frequency of (a) 10 Hz and (b) 15 Hz for the two-layered model using the CBS method.

This equation can be solved iteratively:

$$\begin{aligned}\psi(\mathbf{r}_g, \mathbf{r}_s, k) &= \psi_b(\mathbf{r}_g, \mathbf{r}_s, k_b) \\ &+ k_b^2 \int_D G_b(\mathbf{r}_g, \mathbf{r}')\chi(\mathbf{r}')\psi_b(\mathbf{r}', \mathbf{r}_s)\, d\mathbf{r}' \\ &+ k_b^4 \int_D d\mathbf{r}' G_b(\mathbf{r}_g, \mathbf{r}')\chi(\mathbf{r}') \int_D d\mathbf{r}'' \\ &\times G_b(\mathbf{r}', \mathbf{r}'')\chi(\mathbf{r}'')\psi_b(\mathbf{r}'', \mathbf{r}_s) + \cdots \quad (9)\end{aligned}$$

After taking the first-order term of the conventional Born series, we have the Born approximation:

$$\begin{aligned}\psi(\mathbf{r}_g, \mathbf{r}_s, k) &= \psi_b(\mathbf{r}_g, \mathbf{r}_s, k) \\ &+ k_b^2 \int_D G_b(\mathbf{r}_g, \mathbf{r}', k)\chi(\mathbf{r}')\psi_b(\mathbf{r}', \mathbf{r}_s, k)d\mathbf{r}'. \quad (10)\end{aligned}$$

The Born series is the basis for seismic forward and inverse problems. However, because the Born series assumes weak scattering, it can only converge when the scattering potential is weak (Kirkinis 2008; Wu *et al.* 2007). For real applications, the strength of the contrast in the medium is relatively strong. Divergence may occur in media with strong contrasts.

2.3. *Convergent Born series*

This section revisits the equations for the CBS (Osnabrugge *et al.* 2016). Equations are presented for an arbitrary strong medium. The convergent Born series refers to the situation in which the value of the coefficient of each iteration term is less than unity. The key point for modification of the conventional Born series is to introduce a damping parameter ϵ and a preconditioner γ. Here, we review the derivation of the CBS. To this end, we start with the conventional Born series and apply the preconditioner to both sides of the conventional Born series. It should be noted that the damping parameter ϵ, which is related to the attenuation of the wavefields in the background medium, is also important for the convergence.

In operator form, the Born series (9) can be written as follows:

$$\psi = G\chi\psi + GS, \quad (11)$$

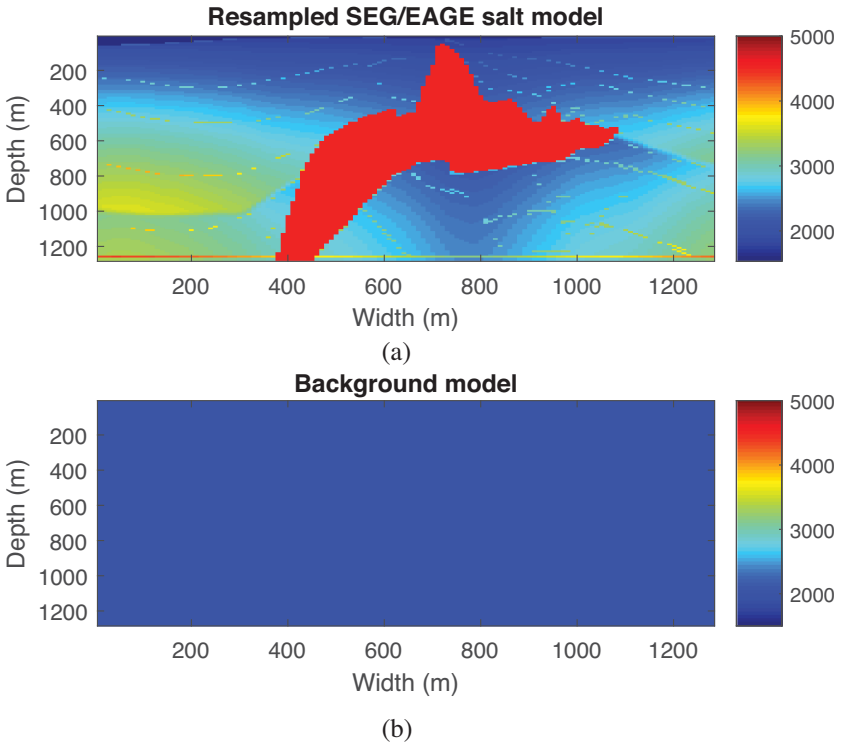

Figure 4. (a) Resampled version of the SEG/EAGE salt model and (b) background model.

where S is the source term, which represents the source wavelet in frequency-space domain, and G is the Green's operator, which represents the Green's function G_b in equation (9). Note that S and ψ are vectors, and G is dense operator filled with various Green's functions. χ is a diagonal matrix. By applying a preconditioner γ to both sides of equation (11), Osnabrugge *et al.* (2016) obtained

$$\gamma\psi = \gamma G\chi\psi + \gamma GS. \tag{12}$$

Then, we reformulate equation (12) as

$$\psi = \Lambda\psi + \gamma GS, \tag{13}$$

with

$$\Lambda = \gamma G\chi - \gamma + 1, \tag{14}$$

where

$$\gamma(\mathbf{r}) = \frac{i}{\epsilon}\chi(\mathbf{r}). \tag{15}$$

The combination of the parameters γ and ϵ can ensure that the largest eigenvalue of Λ is smaller than unity. The details of choice of parameter ϵ will be discussed in the section Implementation. The modified Born series is explained by the following renormalized Born series:

$$\psi = \left(1 + \Lambda + \Lambda^2 + \Lambda^3 + \cdots\right)\gamma GS. \tag{16}$$

The iteration form solution is $\psi = \Lambda\psi + \gamma GS$ with the initial solution $\psi_b = \gamma GS$. The background Green's function can be written as (Osnabrugge *et al.* 2016)

$$G_b(k) = \frac{1}{|k|^2 - k_b^2 - i\epsilon}, \tag{17}$$

and in the real-space domain (Osnabrugge *et al.* 2016)

$$G_b = \frac{e^{i|\mathbf{r}|\sqrt{k_b^2 + i\epsilon}}}{4\pi|\mathbf{r}|}, \tag{18}$$

where k is the wavenumber vector in the real medium.

Because of the introduction of the coefficient of each iteration term Λ and preconditioner γ into the Born series, the modified Born series is convergent. Mathematically, Osnabrugge *et al.* (2016) demonstrated that the modified Born series can converge by combining the two parameters and given the suggestions of choice of the parameters in the optimum scale.

Here, we aim to apply the CBS method to seismic wave modeling problems and provide the renormalization interpretation of the convergent Born series. Due the strong contrast in the seismic problems, it is more challenging. We perform numerical tests and investigate how to choose the coefficient Λ and preconditioner γ for each iteration term, and the dependence on the parameter ϵ. We will look at how the parameter ϵ changes for different models with different strong scattering cases.

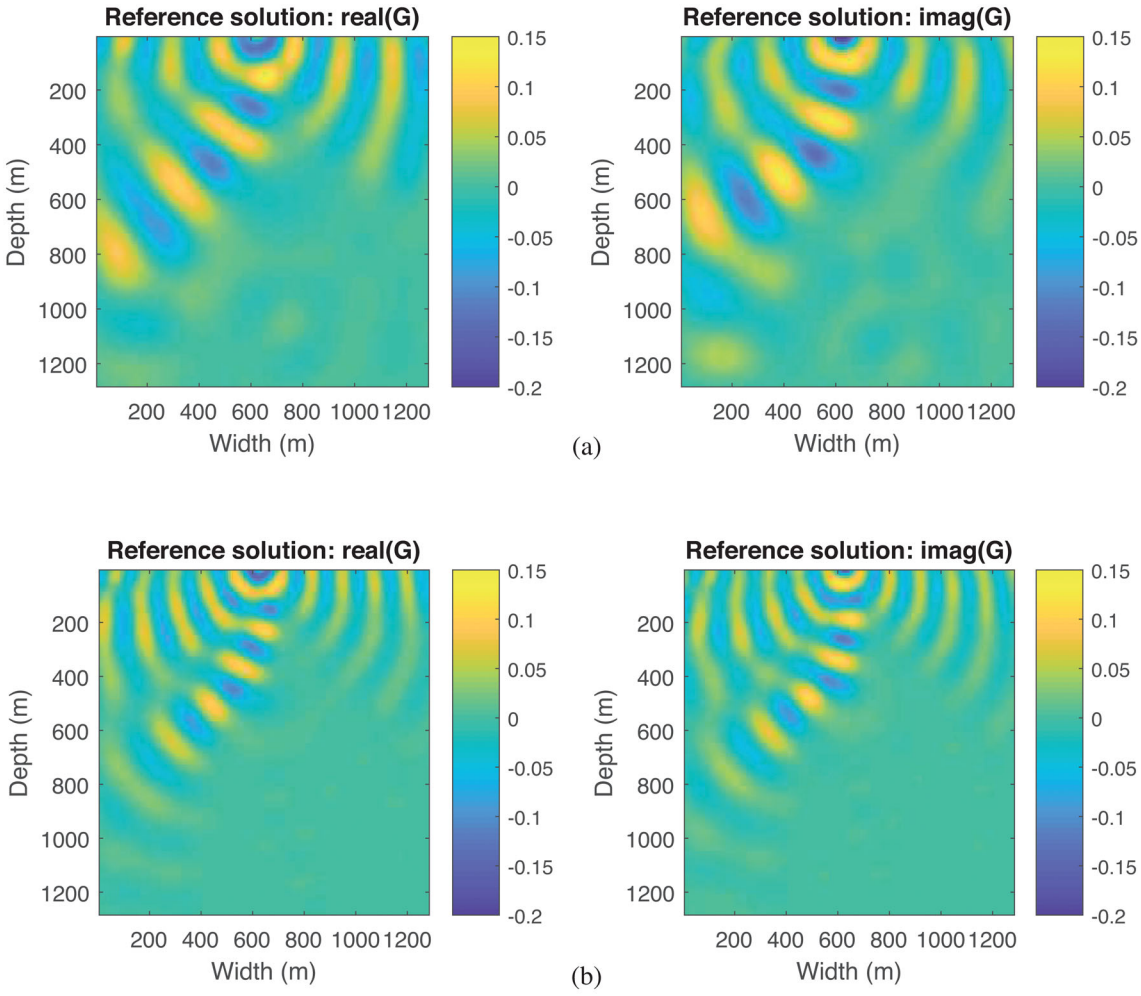

Figure 5. Frequency-domain wavefields for the frequency of (a) 10 Hz and (b) 15 Hz for the SEG/EAGE salt model using the full integral equation method.

3. Interpretation of the convergent Born series

In this section, we discuss the convergent Born series from the renormalization perspective.

3.1. *Step-by-step local interaction*

The modified version of the Born series developed by Osnabrugge *et al.* (2016) is called the convergent Born series. In this modified Born series, a preconditioner γ is introduced. By combining the preconditioner γ and parameter ϵ, the iteration computation satisfies the convergence condition of the Born series.

Actually, the concepts of the locality of wavefields explain how step-by-step propagators prevent the CBS from divergence. From equation (13), we can see that for the conventional Born series, each term involves integrations over the whole volume, which leads to the divergence problems of strongly scattering medium. The CBS makes the total energy in the background medium localized and finite so the volume integral in each term will not blow up. It compensates the damped wavefield by introducing an imaginary part with an opposite sign into the scattering potential V. This means that in the latter procedure the wavefield will grow when interacting with the scattering potential, and therefore compensate the energy loss during propagation in the background medium. In this way, those interactions always act locally, and thus can be regarded as short-range interactions. The iterations will continue until the wavefields cover the whole region with accepted accuracy. Physically, this can be explained as the renormalization process. According to Wilson's RG theory, one can first integrate out the local interactions and then derive the effective action operator, and then go to the next level to calculate the local interactions based on the effective interaction operator. The RG procedure in CBS is more like the mathematician's renormalization procedure

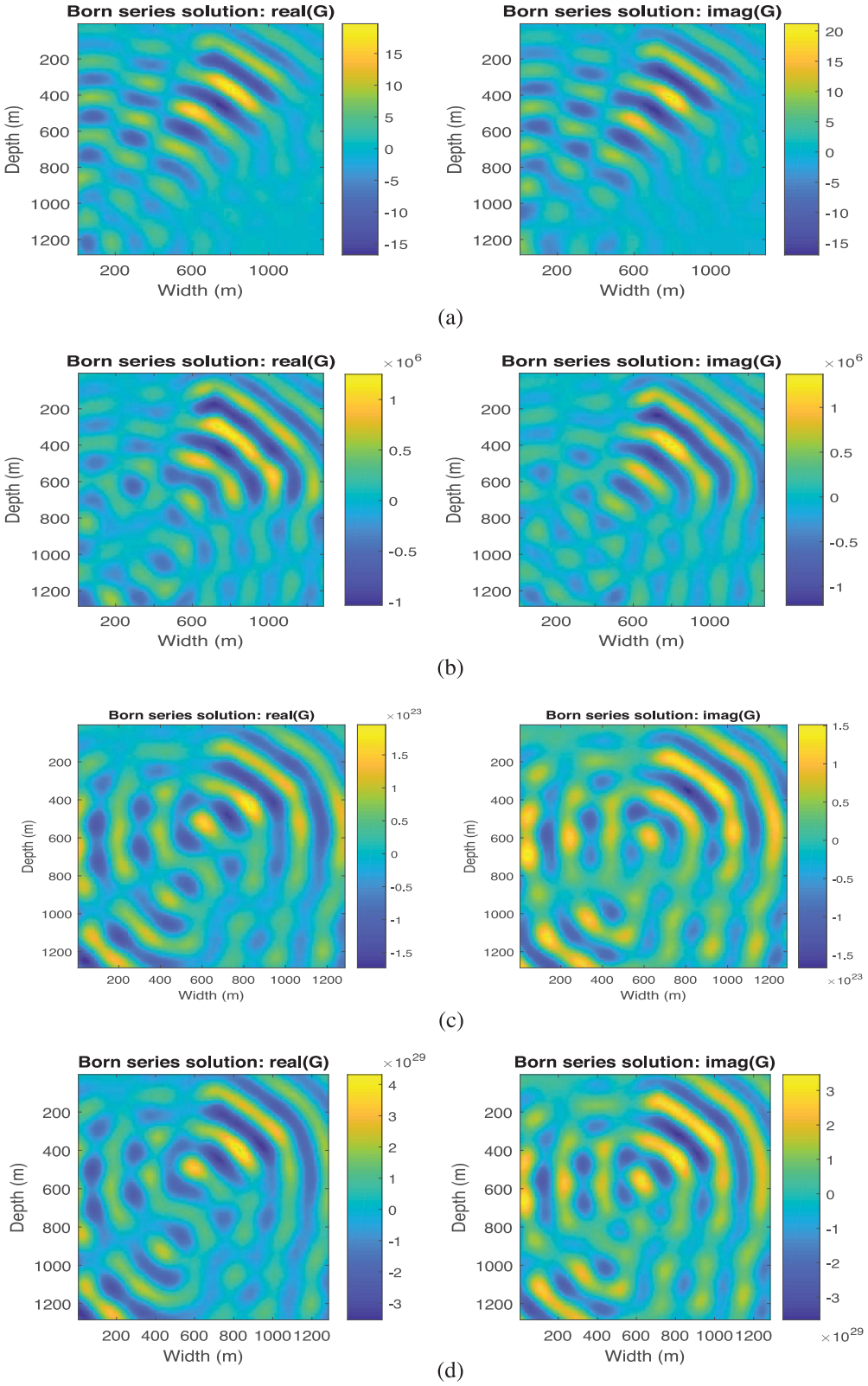

Figure 6. Frequency-domain wavefields with the frequency of 10 Hz for the SEG/EAGE salt model using the BS method with (a) 20, (b) 50, (c) 80 and (d) 100 iterations.

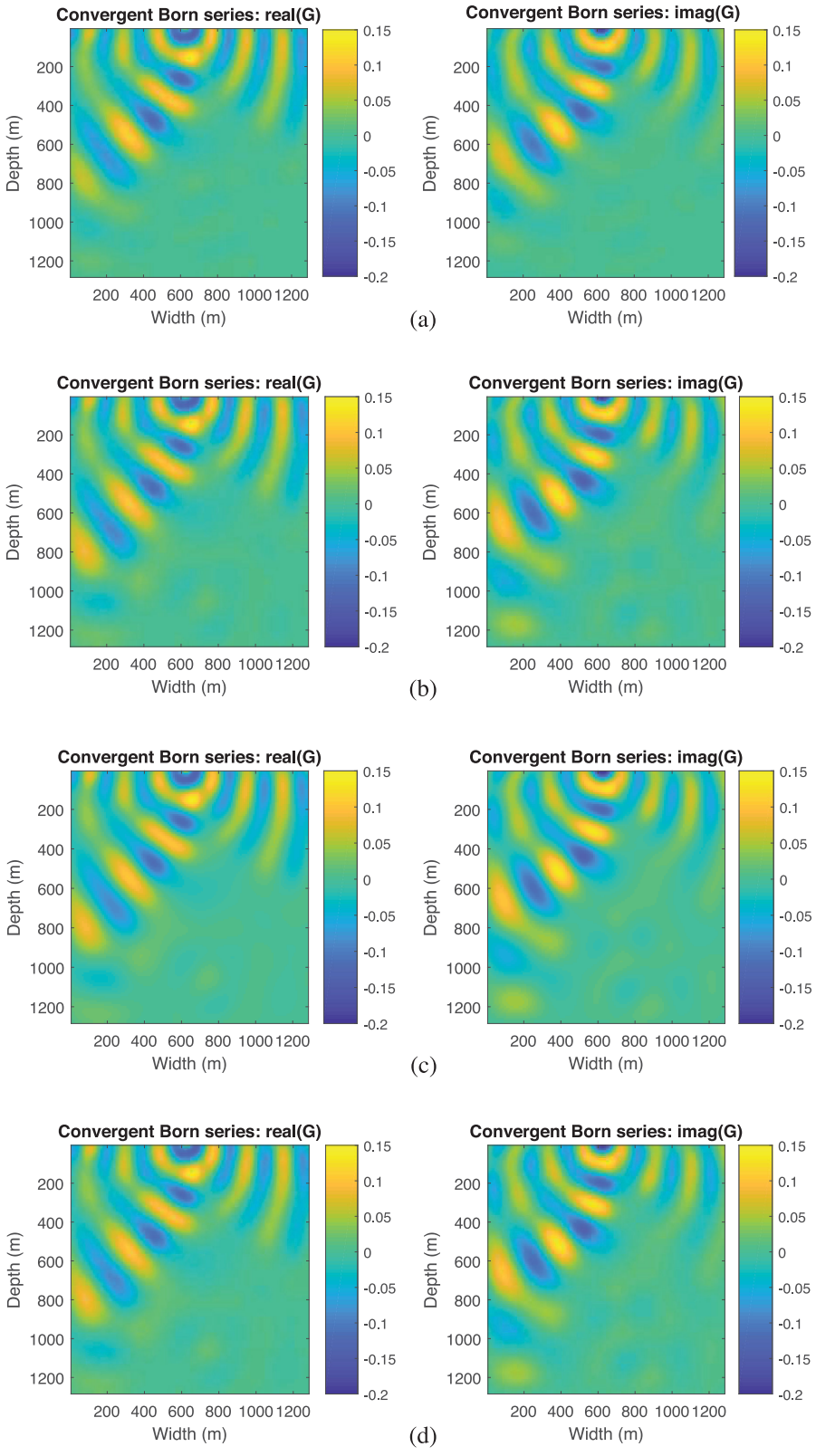

Figure 7. Frequency-domain wavefields with the frequency of 10 Hz for the SEG/EAGE salt model using the CBS method with (a) 20, (b) 50, (c) 80 and (d) 100 iterations.

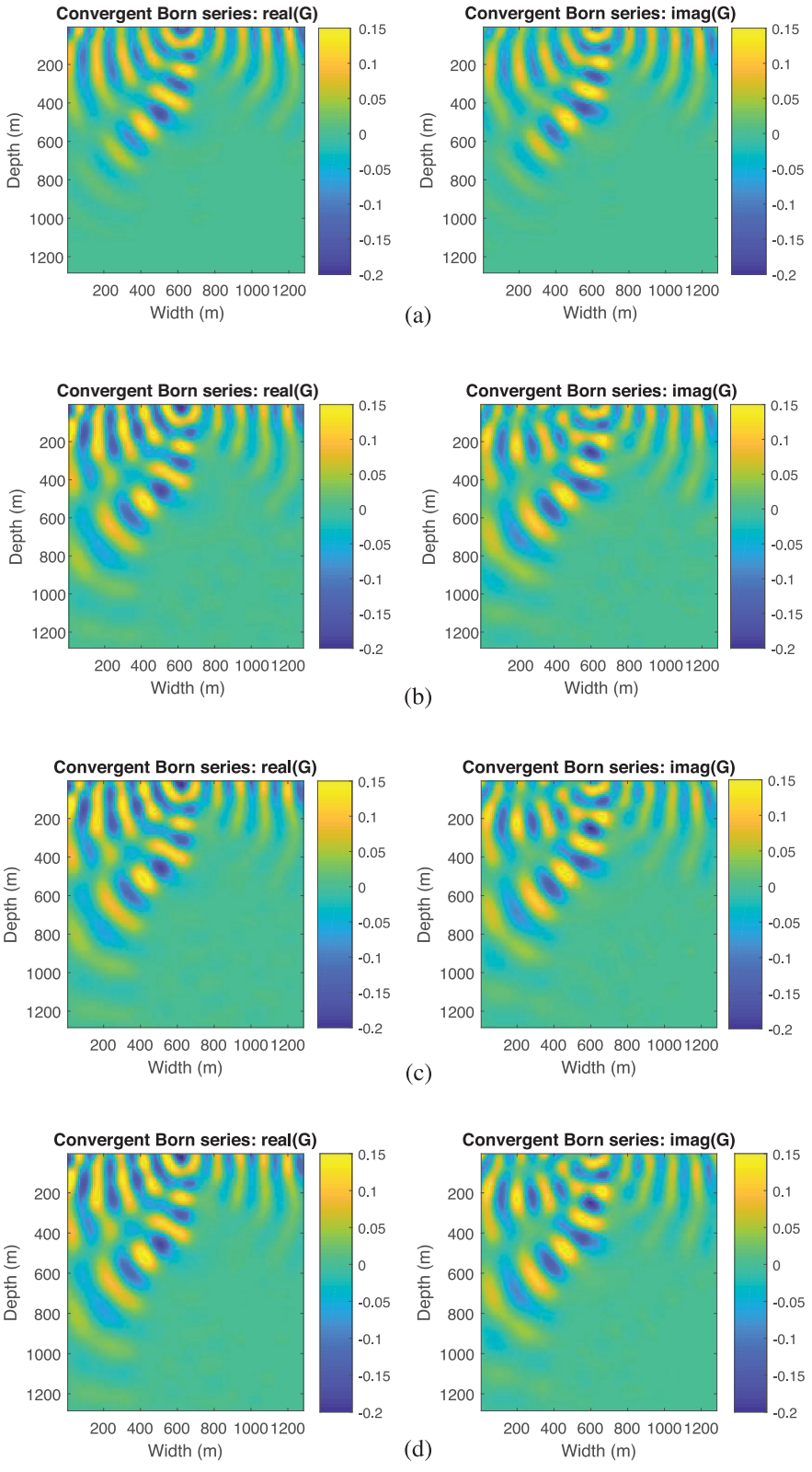

Figure 8. Frequency-domain wavefields with the frequency of 15 Hz for the SEG/EAGE salt model using the CBS method with (a) 20, (b) 50, (c) 80 and (d) 100 iterations.

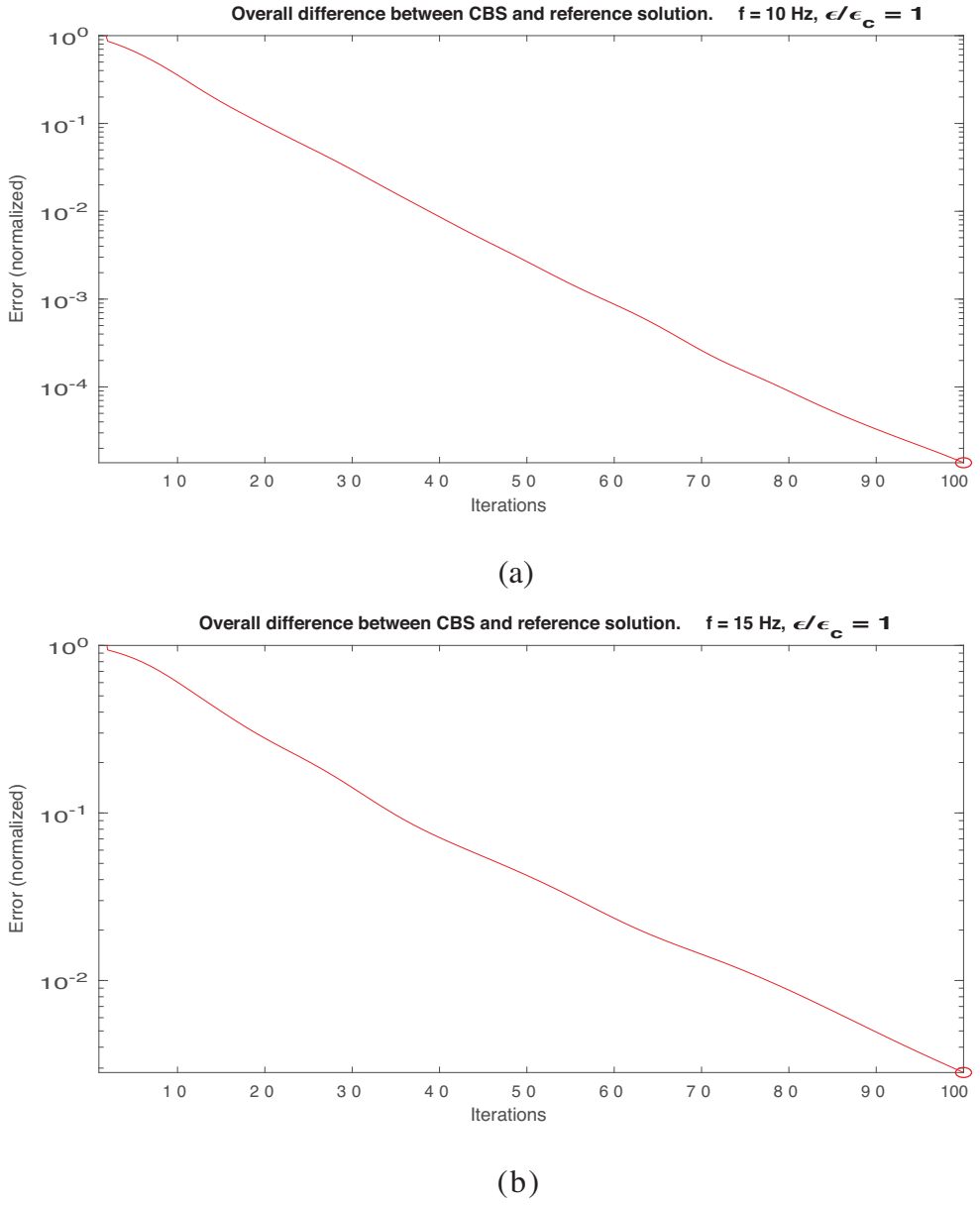

Figure 9. Convergence property of the CBS for the (a) 10 Hz and (b) 15 Hz simulations of the two-layer model.

(Chen *et al.* 1996) using RG theory as a floating initial condition. At each step, the calculated field is treated as a new initial wavefield for further propagation. This is different from Wilson's multi-scale RG procedure.

4. Implementation

In this section, we give the coordinate representation for the CBS. The advantage of this representation is that it is easy to relate two adjacent scattering potentials. Using the coordinate representation, equation (13) can be rewritten as

$$\psi(\mathbf{r}) = \gamma(\mathbf{r})\,\mathrm{G}(\mathbf{r})\,\mathrm{S} + \Lambda(\mathbf{r},\mathbf{r}')\,\psi(\mathbf{r}). \tag{19}$$

The entire model is discretized into $N_x \times N_z$ in the two-dimensional case. Then, we have

$$\psi_{m,n}(\mathbf{r}) = \gamma(\mathbf{r})\,\mathrm{G}_{m,n}(\mathbf{r})\,\mathrm{S} + \sum_{m=1}^{N_x}\sum_{n=1}^{N_z}\Lambda_{m,n}(\mathbf{r},\mathbf{r}')\,\psi_{m,n}(\mathbf{r}), \tag{20}$$

where $i = 1,\ldots,N_x$ and $j = 1,\ldots,N_z$.

It should be noted that, to compute the wavefields at the receivers along the surface, we need to compute the wavefields from the sources to any subsurface point and the background Green's functions from receivers to any subsurface point. For computing the wavefields at any subsurface point, we need compute the wavefields in the background

medium and the Green's functions from any subsurface point to any subsurface point (the Green's function from volume to volume G_{VV}). Then we need compute Λ, which is used for the high-order terms of the CBS. The workflow for implementing the renormalized Born series can be found in Algorithm 1.

Algorithm 1 Pseudo code for renormalized Born series

Initialisation: frequency, maximum iteration number $N_{\max}$ and the parameter ϵ
$m =$ **true model,** $m_0 =$ **background model;**
for $n = 0$ **to** $n = N_{\max}$ **do**
$\chi = k^2 - k_0^2 - i\epsilon$
$kb = \sqrt{k_0^2 + i\epsilon}$
$n = n + 1$
if $n == 0$ **then**
$G_{VV}^{(b)} = Green(VV, kb)$
$G_{VS}^{(b)} = Green(VS, kb)$
$G_{VR}^{(b)} = Green(VR, kb)$
$\psi^{(b)} = GS$
end
$\gamma(\mathbf{r}) = \frac{i}{\epsilon}\chi(\mathbf{r})$
$\Lambda = \gamma G_{VV}\chi - \gamma + 1$
$\psi = \Lambda\psi + \gamma G_{VS}S$
dr=Error $(\psi_{CBS}, \psi_{FullIntegral})$
end for

5. Choice of parameter ϵ in the scale of seismic modeling

An important issue for the CBS is to choose the parameter ϵ. From the analysis in the above section, it can be found that the stronger the scatters (large-contrast), the higher the required parameter ϵ. This is because to eliminate the divergence the wavefields should be strongly localized. From equation (19), one can see that the higher the parameter ϵ, the stronger the attenuation of the background Green's functions. This means that there is a compromise between the demand on the convergence of the CBS and the computational cost. After conducting numerical tests, we find that the parameter ϵ should be chosen as follows:

$$\epsilon = 0.1 \times \max|k^2 - k_b^2| \qquad \text{if} f < 3, \tag{21}$$

and

$$\epsilon = \max|k^2 - k_b^2| \qquad \text{if} f > 3. \tag{22}$$

After investigating the convergence of the convergent Born series, Fast-Fourier Transform (FFT) is used, which can accelerate the computation in the implementation. Following Osnabrugge *et al.* (2016), we employ the FFT technique for an efficient matrix-free implementation. The FFT method has been used for integral equation modeling (Liu *et al.* 2001; Gao & Torres-Verdin 2006). The matrix–vector multiplications can be expressed as

$$\mathrm{G}\chi = \mathcal{F}^{-1}[\mathcal{F}[\mathrm{G}]\mathcal{F}[\chi]], \tag{23}$$

where $\mathcal{F}$ is the forward 2D FFT operator and $\mathcal{F}^{-1}$ is the inverse 2D FFT operator. It should be noted that the product is performed in the size of $2N_x \times 2N_z$. The computational complexity is $O[N_xN_z log(N_xN_z)]$ and the memory complexity is $O[N_xN_z]$.

6. Synthetic results

6.1. Comparison of frequency-domain wavefields

In this section, we share the frequency-domain wavefields for different models, including two-layers and the SEG/EAGE salt models as well as, compare the convergence property of the CBS by calculating the normalized errors and share the pressure response along receiver line for different iterations. To demonstrate the accuracy of the CBS, we compare it with the full integral equation method (Jakobsen & Wu 2016). We have used homogeneous background media in the tests and the velocity is 2000 m s^{-1}.

We first compare the renormalized Born series against the T-matrix method in an acoustic two-layer model (figure 1). The model measures 1280 m × 1280 m with grid intervals for the simulations of 10 m × 10 m.

Snapshots of frequency-domain wavefields computed with the full integral equation method and the convergent Born series are shown in figures 2 and 3, respectively. In each figure, we show the wavefields of two frequencies, 10 Hz and 15 Hz. From figures 2 and 3, one can make the following observations: (1) the wavefields using all the methods display an obvious change around the boundary; (2) the wavefields using the CBS match well with those from the reference integral equation method.

Figure 4 shows the resampled SEG/EAGE salt model for this example. The model grid is 10 m × 10 m. The model represents a uniform mesh of 128 × 128 nodes. We have performed simulations of frequency-domain wavefields in which the frequencies of 10 Hz and 15 Hz are used. Figure 5 shows the wavefields for 10 Hz and 15 Hz obtained by the reference integral equation method with 100 iterations. Figure 6 shows the wavefield snapshots for 10 Hz obtained by the conventional Born series (BS) method with 20, 50, 80 and 100 iterations. Figures 7 and 8 show the wavefields at frequencies 10 Hz and 15 Hz, respectively, obtained by the CBS method with 20, 50 ,80 and 100 iterations. From figures 5, 7 and 8, one can observe that the results from the CBS method have a good match with the results from full integral

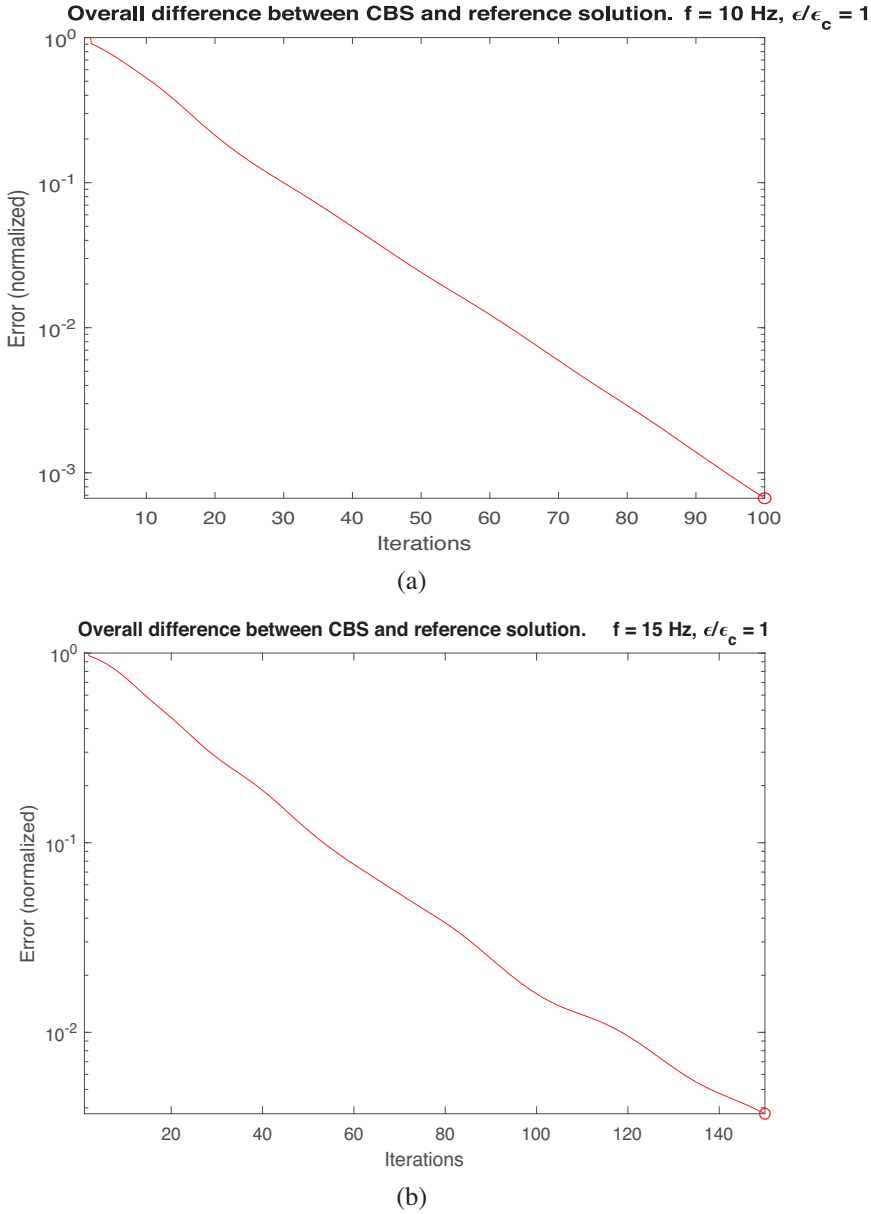

Figure 10. Convergence property of the CBS for (a) 10 Hz and (b) 15 Hz simulations of the SEG/EAGE salt model.

equation approach. All computations were performed on an Intel i7-7700. The CPU of the computer is 3.60 GHz with RAM 64 GB. The computational times of the full integral equation and CBS for 100 iterations are 859 s and 492 s, respectively.

6.2. *Convergence property of the CBS*

To investigate the convergence property of the CBS, we calculate the normalized error. Figures 9 and 10 show the results for the two-layered and the SEG/EAGE salt models, respectively . The figures show that the CBS has a similar convergence property in different models and frequencies, but the error decreases in a different way. With the same iterations, the error in the two-layered model is smaller than those of the SEG/EAGE salt model. From the figures, one can observe that after around 100 iterations the error of the CBS is very small. This suggests that the CBS can give a good match with the reference solution.

6.3. *Frequency-domain wavefields with FFT*

Because we use FFT in the implementation, some periodic boundary condition problems may occur (Osnabrugge *et al.* 2016). To prevent the reflection from the boundaries, we use an absorbing boundary condition in the implementation

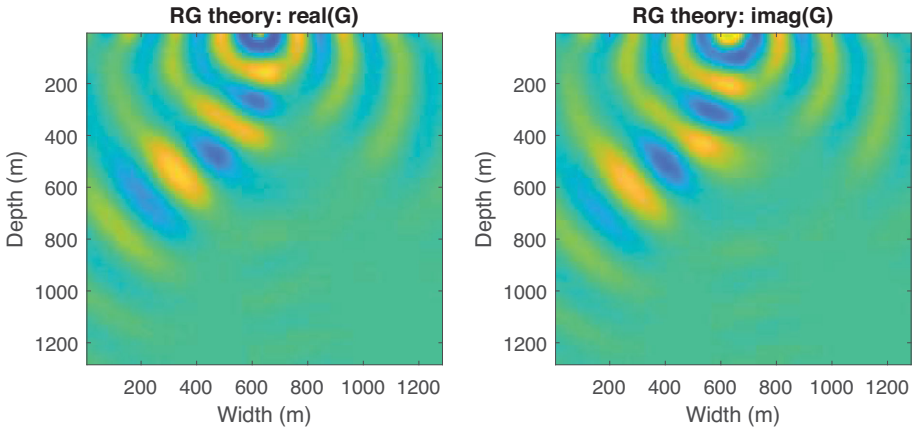

Figure 11. Frequency-domain wavefields for 10-Hz simulation of SEG/EAGE model using the CBS with FFT.

of the CBS. The absorbing boundary condition has been used in the context of wave modeling by different authors. More specifically, for the CBS, we use a width of absorbing boundary layer with grids of 40×40. Figure 11 shows the frequency-domain wavefields of 10 Hz using the CBS with FFT. We have estimated the computational cost. The computational times of the reference integral equation method is 492 s. The computational time of the CBS with FFT is 100 s.

6.4. Anomalous pressure response along receiver line

We now consider the same simulation as the SEG/EAGE salt models but for the synthetic pressure response along the receiver line. This example is designed to test the accuracy of the numerical scheme. Figure 12 shows the results for a two-layered model, in which the frequencies of 10 Hz and 15 Hz are used. Figures 13 and 14 show the pressure response in a salt model using the BS method with the frequency of 10 Hz for different iterations. Figures 15 and 16 show the pressure using the CBS method with the frequency of 10 Hz for the salt model. Figures 17 and 18 show the pressure using the CBS method with the frequency of 15 Hz for the salt model. For all the tests, the point source is placed at the same position. A receiver line is located at the surface. From figures 13 and 14, one can observe that the results from the BS method do not agree with the pressure wavefields from the full integral equation method. From figures 15–18, we observe that the pressure response using the CBS works very well compared with the result using the reference integral equation method.

7. Discussion

Before we discuss the convergence, computational complexity and potential application of the CBS, we would like to clarify that we have presented the theory and performed the numerical tests in the frequency domain because scattering theory is naturally formulated in the frequency domain and we do not have to generate time-domain waveforms to perform inversion in the frequency domain. The main reason for using a homogeneous reference medium is that we want to use FFT, which depends on the fact that the Greens function for a homogeneous medium is directly related to the difference between x and x'. Another point is that the contrast is frequency-dependent. In our tests, we used different frequencies and investigated different choices of parameter ϵ.

The application of the BS to seismic forward modeling requires small contrasts to achieve convergence. Here, by applying a preconditioner to the both sides of the BS and introducing the parameter ϵ to the background Green's function, the convergence of the BS is guaranteed. Figures 19 and 20 show the difference of frequency-domain wavefields for SEG/EAGE salt model using full integral equation and CBS methods. Osnabrugge *et al.* (2016) have already provided a general proof of convergence, we have used numerical examples to verify that the general proof holds for our specific models. However, for the case where the contrast is very large, e.g. salt areas, more iterations are needed to achieve convergence. This is also related to the choice of the parameter ϵ. The stronger the scatters (large-contrast), the higher the needed parameter ϵ.

Compared to the conventional BS there is no additional computational cost for each term in the real-space implementation. It should be noted that the accuracy of the wavefields depend on the number of iteration. This is different from the full IE method. One important thing we would like to mention is that, due to the FFT implementation for the CBS, the computational cost is reduced significantly. The computational complexity for such an implementation

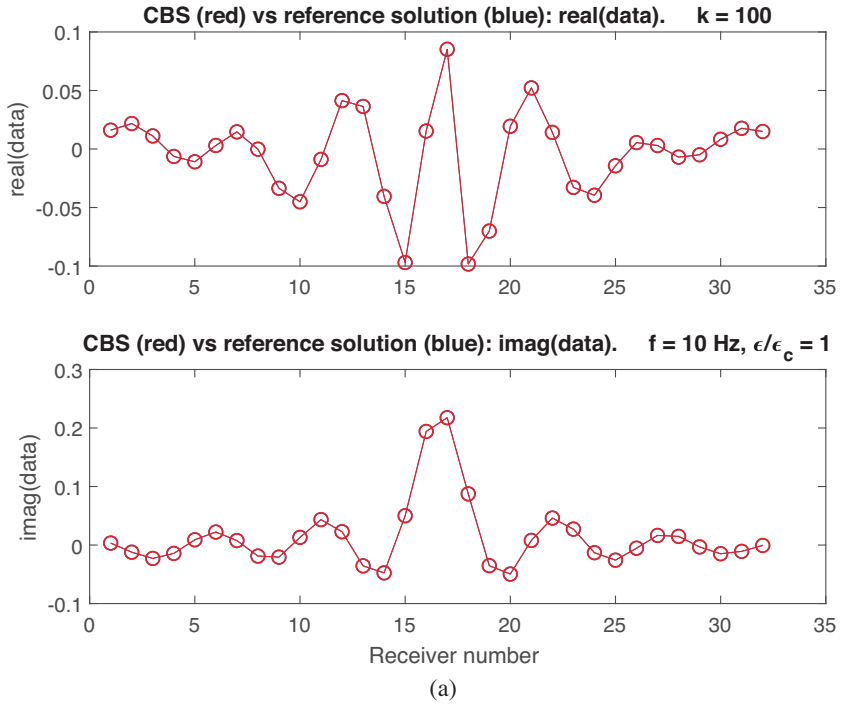

(a)

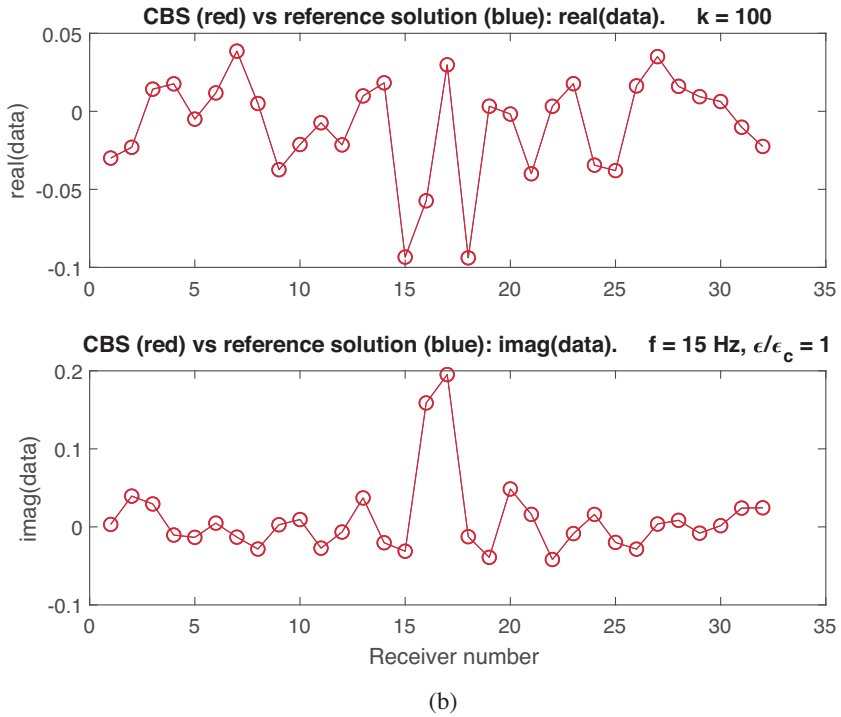

(b)

Figure 12. Comparison of pressure records for the two-layer model using the CBS and full integral equation methods with the frequencies of (a) 10 Hz and (b) 15 Hz, respectively.

is $O[N_x N_z log(N_x N_z)]$ and the memory complexity is $O[N_x N_z]$. Thus, the method can be in principle extended to the 3-D case.

We have presented and tested a new forward scattering series for seismic modeling. The method is suitable for numerical simulation of strongly scattering medium. The scattering series can be used for direct inverse scattering problems. Future research can look into the application of the CBS to the elastic case as well as in seismic inversion. The CBS in this paper can be considered as a stepping

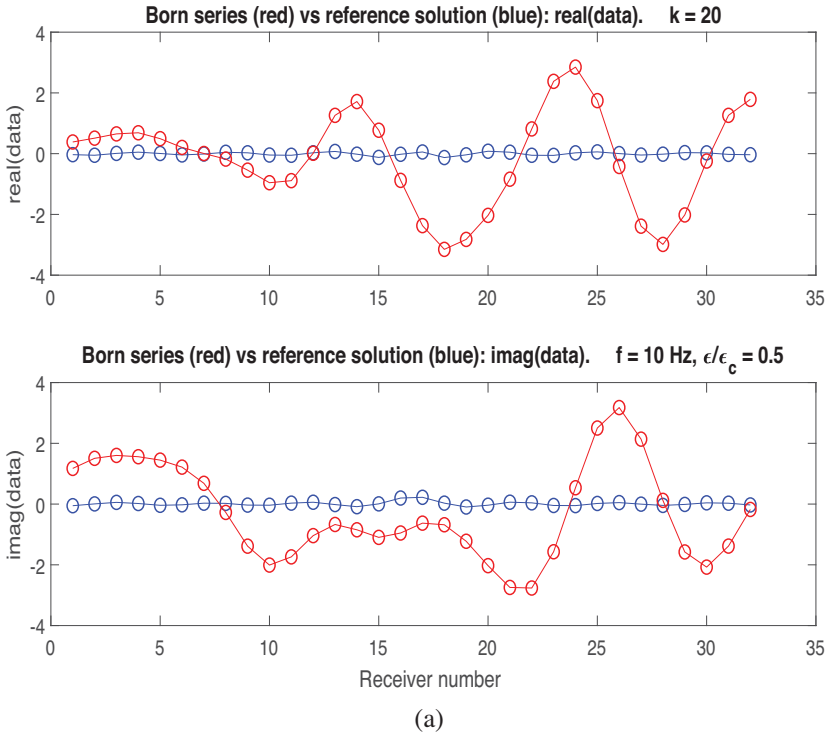

(a)

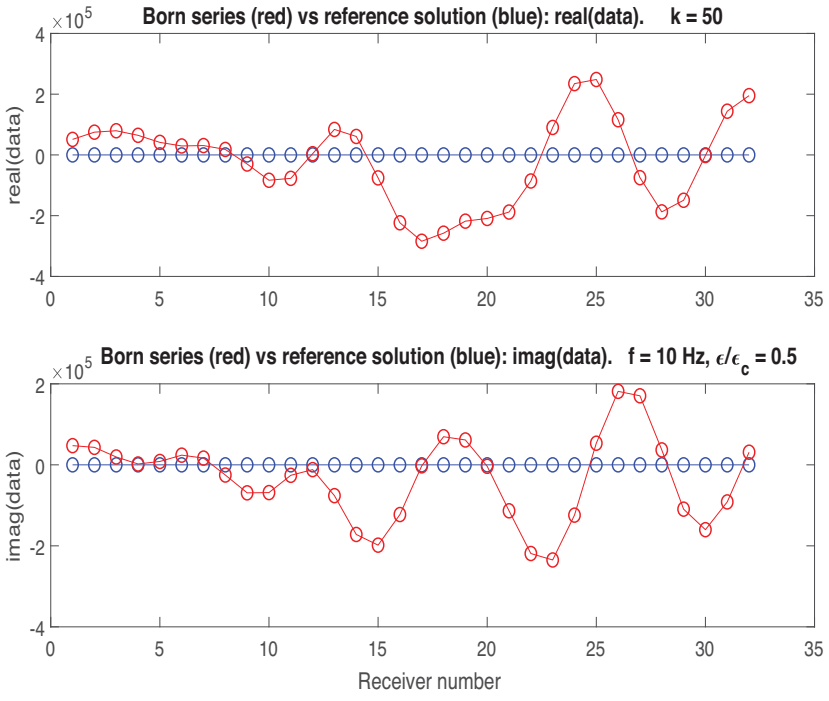

(b)

Figure 13. Comparison of pressure records for the SEG/EAGE salt model using the BS and full integral equation methods with the frequency of 10 Hz with a) 20, b) 50 iterations.

stone to developing modifications for one-way propagators. Also, it can be used to establish the Frechet derivatives for multi-scattering full waveform inversion (Alkhalifah & Wu 2016).

8. Conclusions

Seismic scattering theory is an effective method for seismic wave modeling and is the basis of seismic inversion. However, the Born series assumes weak scattering, which

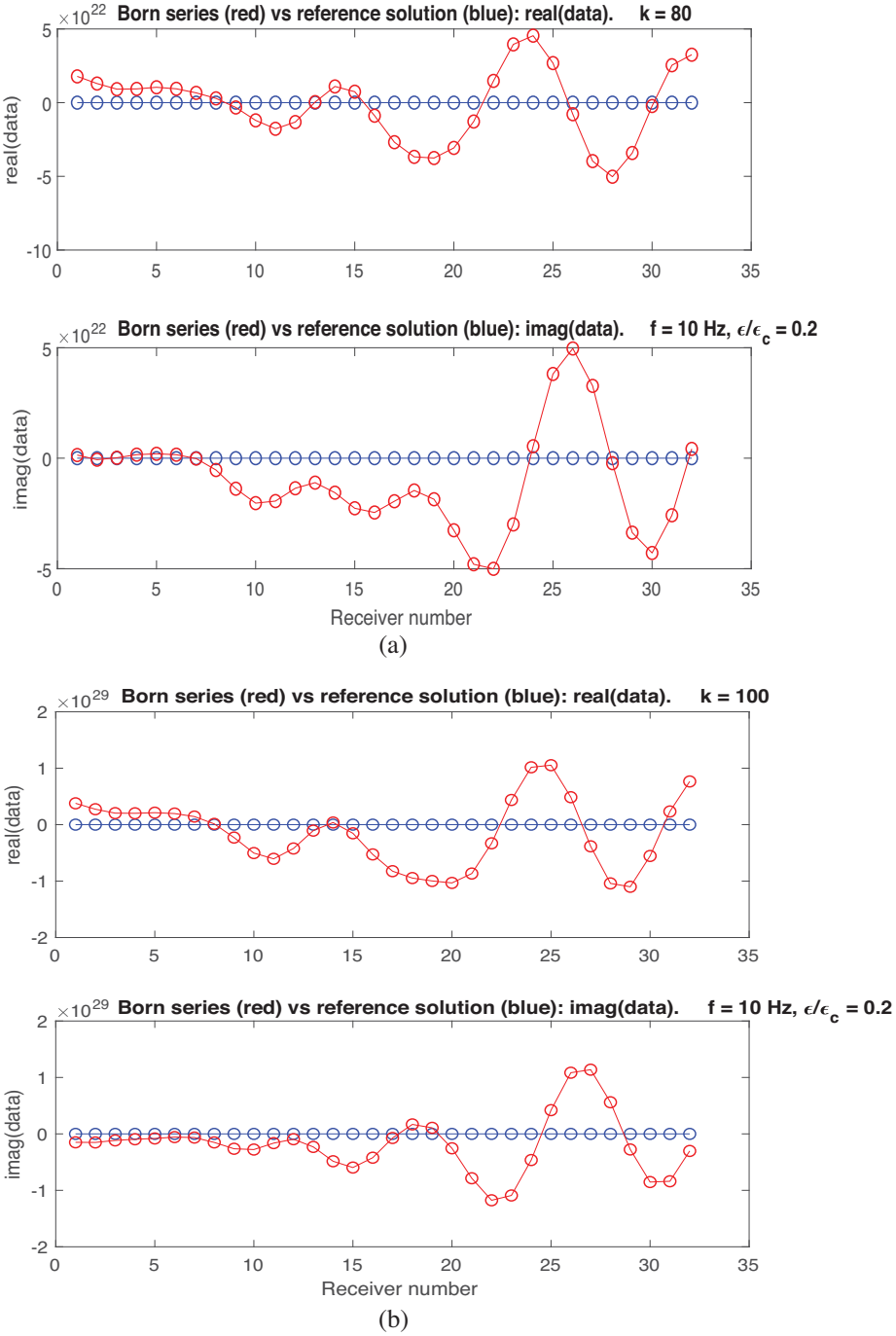

Figure 14. Comparison of pressure records for the SEG/EAGE salt model using the BS and full integral equation methods with the frequency of 10 Hz with (a) 80 and (b) 100 iterations.

renders the modeling and the inversion divergent for strong scattering media. We have presented the application of the so-called convergent Born series to seismic modeling problems. Numerical examples are presented, showing that, because of the introduction of a preconditioner into the traditional Born series, the Born series can be convergent for arbitrarily strong contrast medium. Compared to the integral equation method, the computational cost of the convergent Born series is cheaper, especially in the Fast Fourier Transform implementation. This method should be suitable for applications to inverse scattering and full waveform inversion.

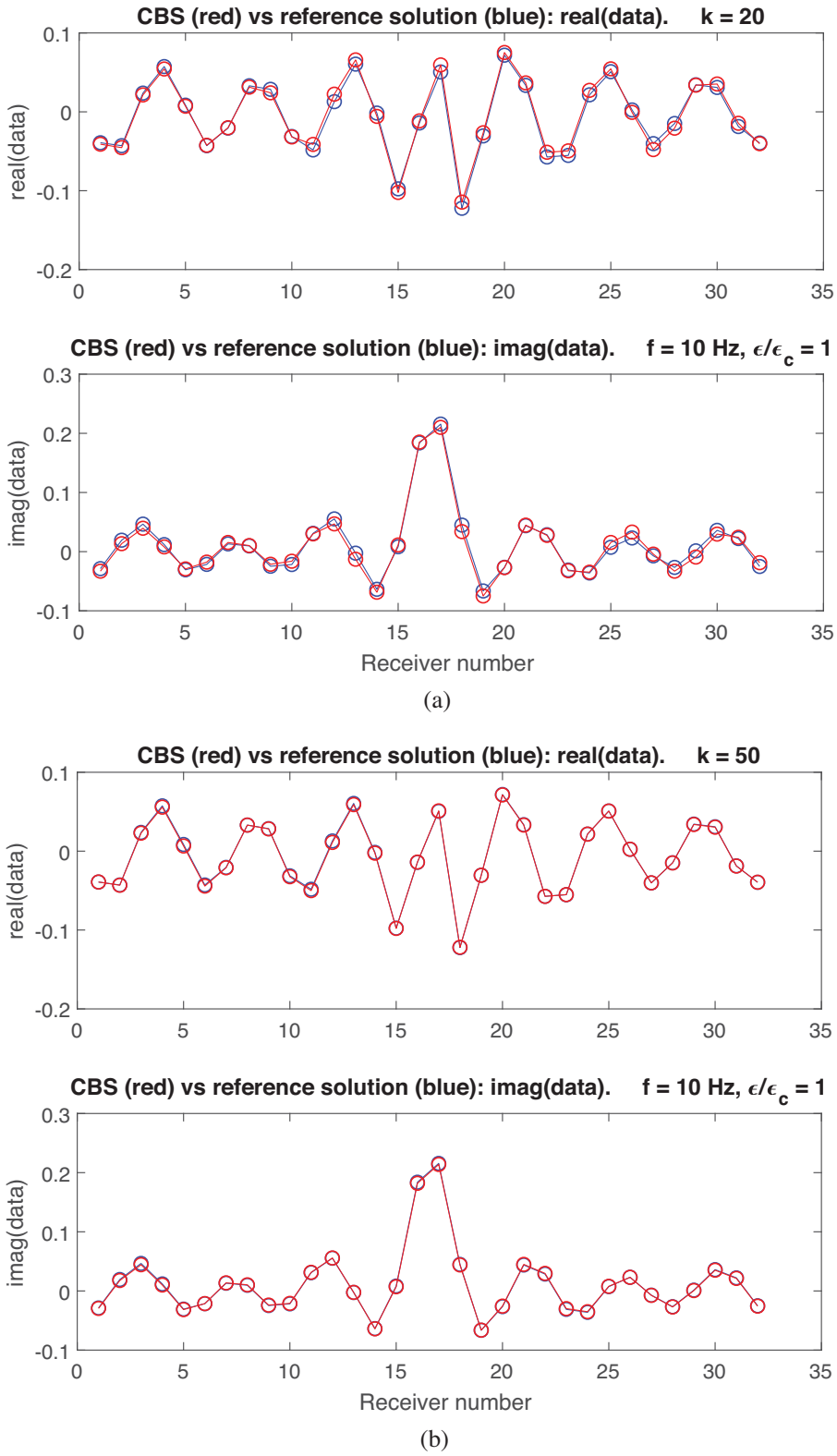

Figure 15. Comparison of pressure records for the SEG/EAGE salt model using the CBS and full integral equation methods with the frequency of 10 Hz with (a) 20 and (b) 50 iterations.

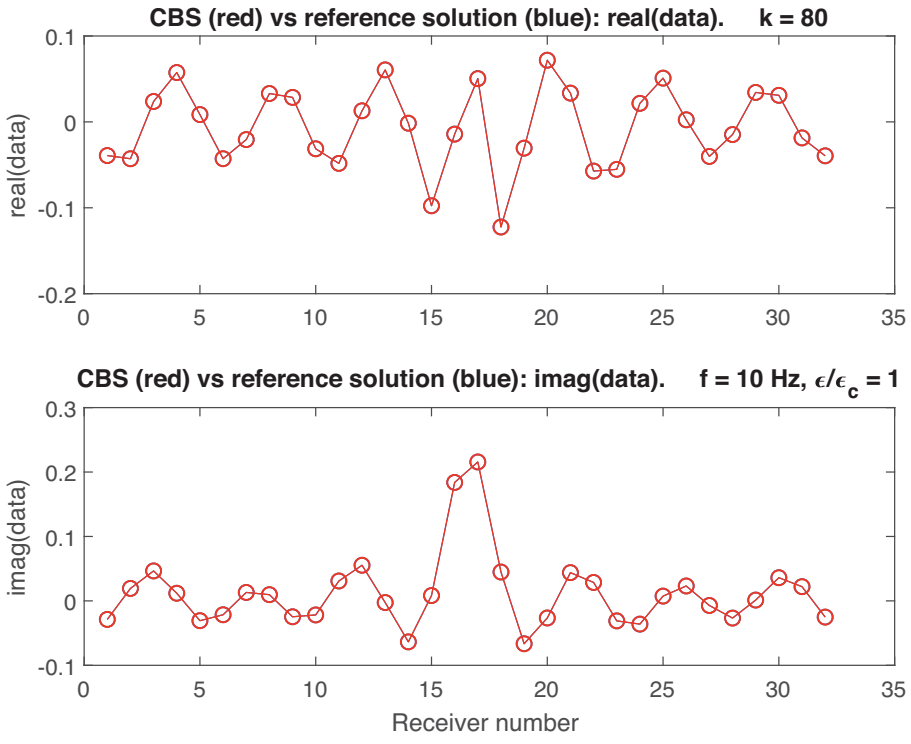

(a)

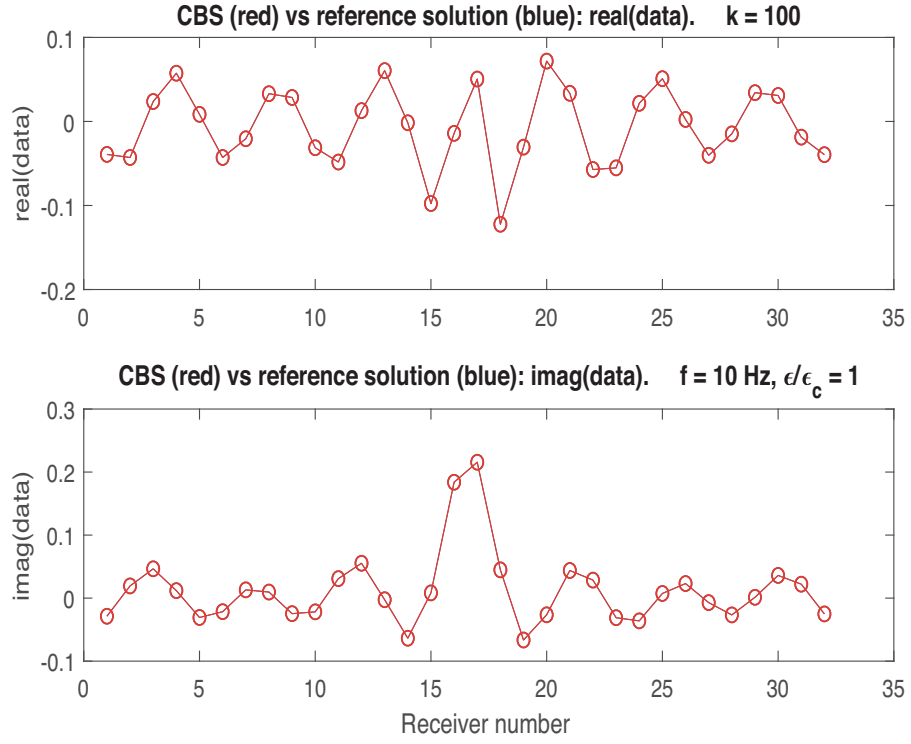

(b)

Figure 16. Comparison of pressure records for the SEG/EAGE salt model using the CBS and full integral equation methods with the frequency of 10 Hz with (a) 80, (b) 100 iterations.

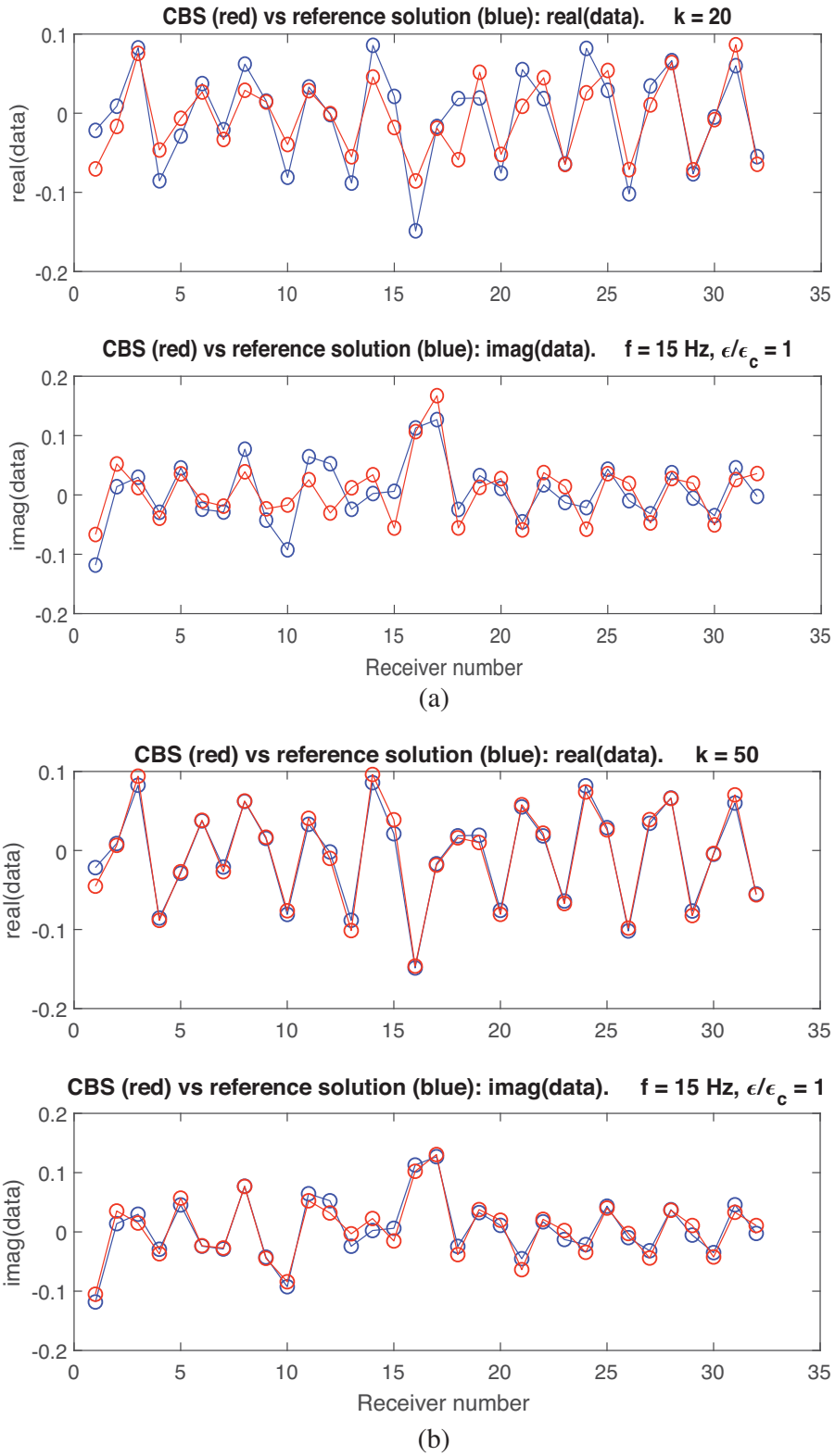

Figure 17. Comparison of pressure records for the SEG/EAGE salt model using the CBS and full integral equation methods with the frequency of 15 Hz with (a) 20, (b) 50 iterations.

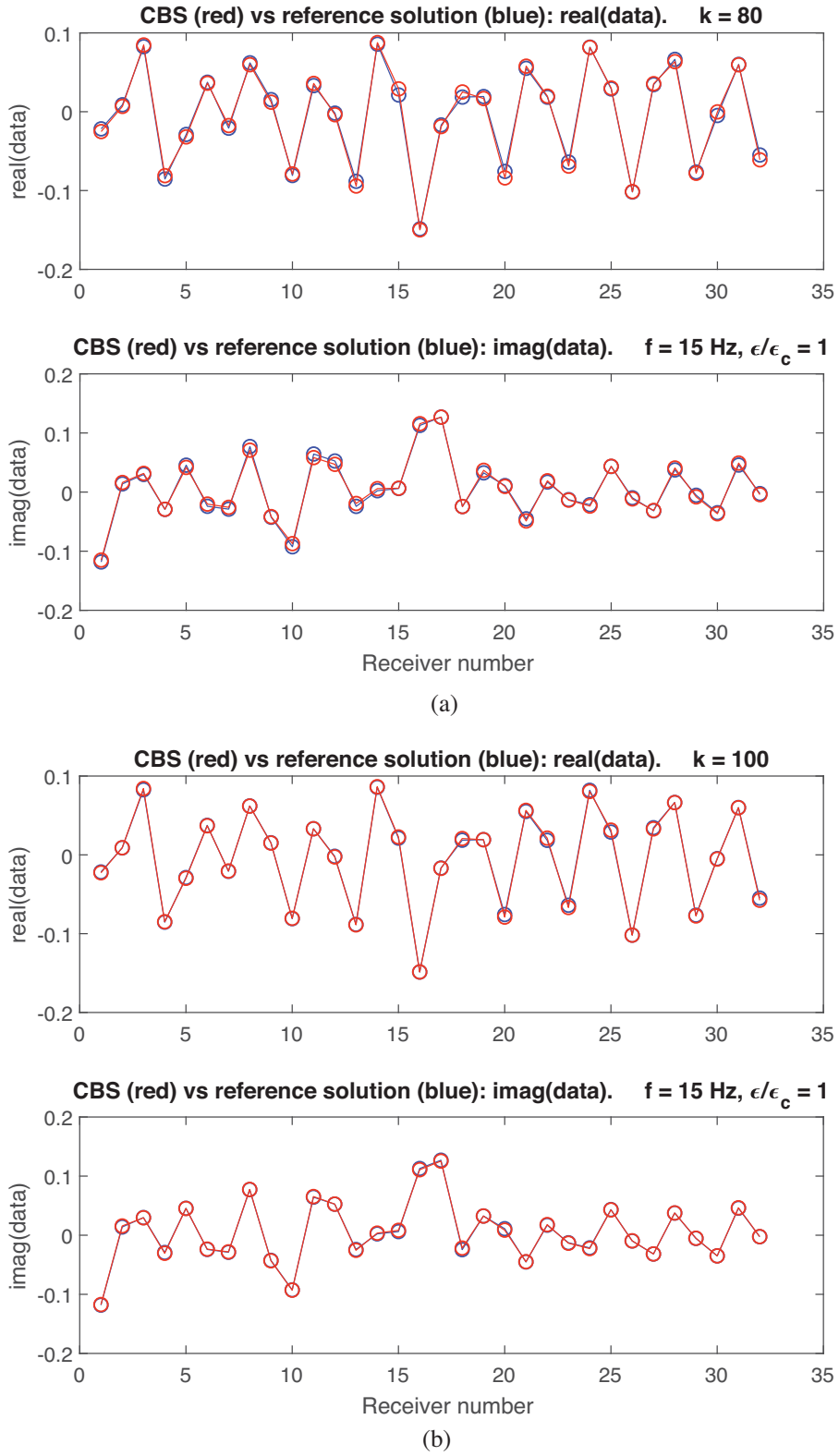

Figure 18. Comparison of pressure records for the SEG/EAGE salt model using the CBS and full integral equation methods with the frequency of 15 Hz with (a) 80 and (b) 100 iterations.

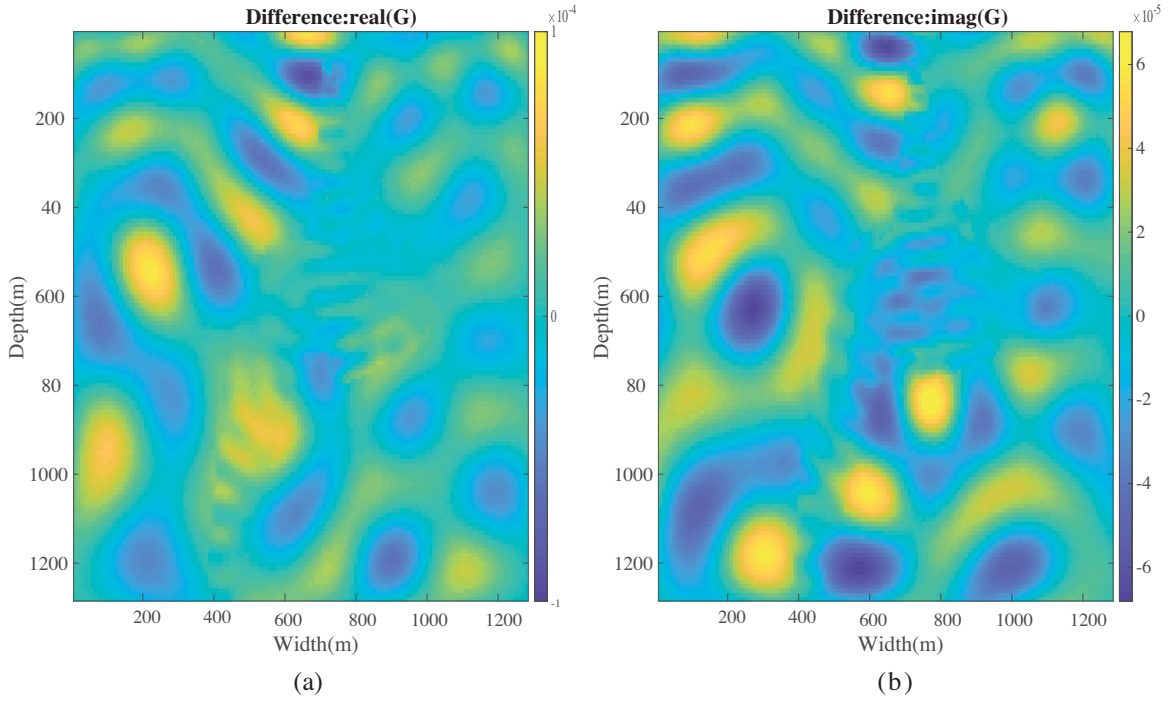

Figure 19. Difference of wavefields of real (a) and imaginary (b) parts using the CBS and full integral equation methods with the frequency of 10 Hz.

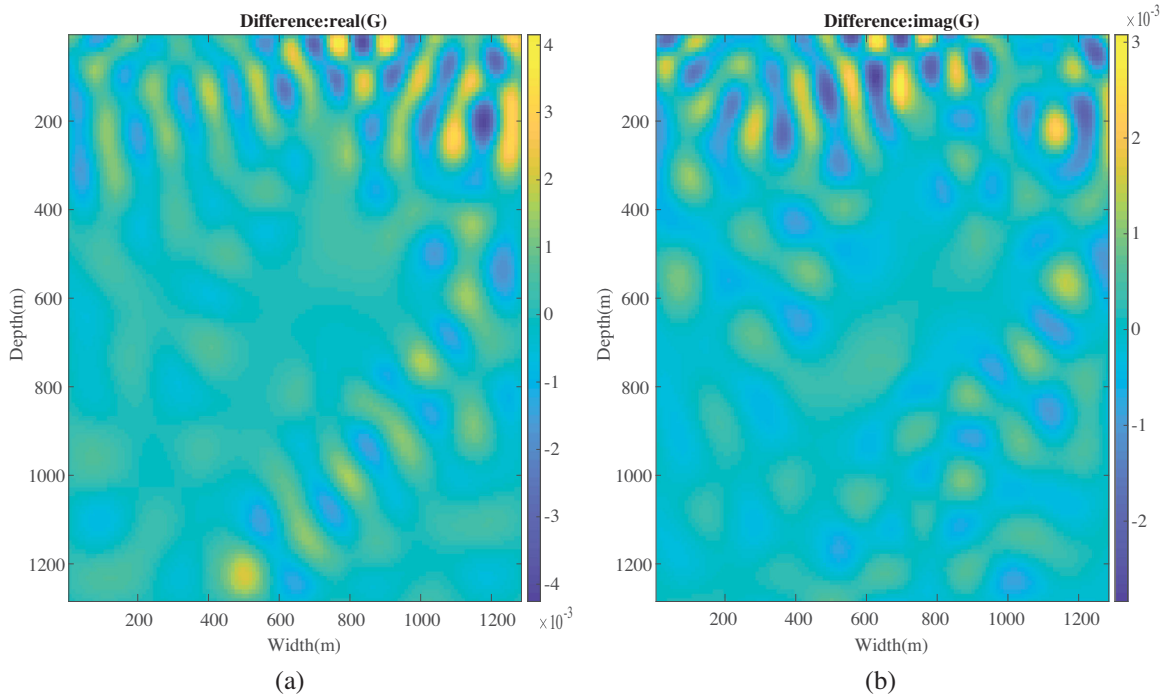

Figure 20. Difference of wavefields of real (a) and imaginary (b) parts using the CBS and full integral equation methods with the frequency of 15 Hz.

Acknowledgements

We thank the Research Council of Norway for the Petromaks II project 267769/E3 (Bayesian inversion of 4D seismic waveform data for quantitative integration with production data). We would like to acknowledge the WTOPI (Wavelet Transform On Propagation and Imaging for seismic exploration) Research Consortium sponsors for their financial support. Furthermore, we are grateful to Gerwin Osnabrugge at University of Twente, for very helpful discussion, the Editor and reviewers for their very constructive comments on the manuscript.

References

Aki, K. & Richards, P.G., 1980. *Quantitative Seismology*, W. H. Freeman and Company, 1st ed., 932, San Francisco, Calif.

Alkhalifah, T., 2016. Full-model wavenumber inversion: An emphasis on the appropriate wavenumber continuation, *Geophysics*, **81**, R89–R98.

Alkhalifah, T. & Wu, Z., 2016. Multiscattering inversion for low-model wavenumbers, *Geophysics*, **81**, R417–R428.

Berkhout, A., 2012. Combining full wavefield migration and full waveform inversion, a glance into the future of seismic imaging, *Geophysics*, **77**, S43–S50.

Carcione, J.M., 2007. *Wave Fields in Real Media: Wave Propagation in Anisotropic, Anelastic, Porous and Electromagnetic Media*, Elsevier.

Cerveny, V., 2005, *Seismic Ray Theory*, Cambridge University Press.

Chen, L.Y., Goldenfeld, N. & Oono, Y., 1994. Renormalization group theory for global asymptotic analysis, *Physical Review Letters*, **73**, 1311–1315.

Chen, L.Y., Goldenfeld, N. & Oono, Y., 1996. Renormalization group and singular perturbations: Multiple scales, boundary layers, and reductive perturbation theory, *Physical Review E*, **54**, 376–394.

De Wolf, D., 1971. Electromagnetic reflection from an extended turbulent medium: cumulative forward-scatter single backscatter approximation, *IEEE Transactions on Antennas and Propagation*, **19**, 254–262.

De Wolf, D., 1985. Renormalization of EM fields in application to largeangle scattering from randomly continuous media and sparse particle distributions, *IEEE Transactions on Antennas and Propagation*, **33**, 608–615.

Delamotte, B., 2004. A hint of renormalization, *American Journal of Physics*, **72**, 170–184.

Eftekhar, R., Hu, H. & Zheng, Y., 2018. Convergence acceleration in scattering series and seismic waveform inversion using nonlinear shanks transformation, *Geophysical Journal International*, **214**, 1732–1743.

Gao, G. & Torres-Verdin, C., 2006. High-order generalized extended Born approximation for electromagnetic scattering, *IEEE Transactions on Antennas and Propagation*, **54**, 1243–1256.

Gell-Mann, M. & Low, F.E., 1954. Quantum electrodynamics at small distances, *Physical Review*, **95**, 1300–1312.

Goldenfeld, N., 1992. *Lectures on Phase Transition and the Renormalization Group*, Addison-Wesley.

Huang, X., 2018. Extended beam approximation for high frequency wave propagation, *IEEE Access*, **6**, 37214–37224.

Huang, X. & Greenhalgh, S., 2019. Traveltime approximation for strongly anisotropic media using the homotopy analysis method, *Geophysical Journal International*, **216**, 1648–1664.

Huang, X., Jakobsen, M., Naevdal, G. & Eikrem, K.S., 2019. Target-oriented inversion of time-lapse seismic waveform data, *Communications in Computational Physics*, doi:10.4208/cicp.OA-2018-0143.

Huang, X., Sun, H. & Sun, J., 2016a. Born modeling for heterogeneous media using the gaussian beam summation based Green's function, *Journal of Applied Geophysics*, **131**, 191–201.

Huang, X., Sun, J. & Sun, Z., 2016b. Local algorithm for computing complex travel time based on the complex eikonal equation, *Physical Review E*, **93**, 043307.

Huang, X., Sun, J. & Greenhalgh, S., 2018. On the solution of the complex eikonal equation in acoustic vti media: a perturbation plus optimization scheme, *Geophysical Journal International*, **214**, 907–932.

Innanen, K.A., 2009. Born series forward modelling of seismic primary and multiple reflections: an inverse scattering shortcut, *Geophysical Journal International*, **177**, 1197–1204.

Jakobsen, M. & Wu, R., 2016. Renormalized scattering series for frequency-domain waveform modelling of strong velocity contrasts, *Geophysical Journal International*, **206**, 880–899.

Jakobsen, M., Wu, R.S. & Huang, X., 2018. Seismic waveform modeling in strongly scattering media using renormalization group theory, *SEG Technical Program Expanded Abstracts 2018*, **1**, 5007–5011.

Kirkinis, E., 2008. Renormalization group interpretation of the Born and Rytov approximations, *Journal of the Optical Society of America A*, **25**, 2499–2508.

Kirkinis, E., 2012. The renormalization group: a perturbation method for the graduate curriculum, *SIAM Review*, **54**, 374–388.

Kouri, D.J. & Vijay, A., 2003. Inverse scattering theory: Renormalization of the Lippmann–Schwinger equation for acoustic scattering in one dimension, *Physical Review E*, **67**, 046614.

Liu, Q.H., Zhang, Z.Q. & Xu, X.M., 2001. The hybrid extended Born approximation and CG-FFT method for electromagnetic induction problems, *IEEE Transactions on Geoscience and Remote Sensing*, **39**, 347–355.

Malovichko, M., Khokhlov, N., Yavich, N. & Zhdanov, M., 2017. Approximate solutions of acoustic 3D integral equation and their application to seismic modeling and full-waveform inversion, *Journal of Computational Physics*, **346**, 318–339.

Morse, P.M. & Feshback, H., 1953. Methods of theoretical physics, McGraw-Hill Science/Engineering/Math.

Osnabrugge, G., Leedumrongwatthanakun, S. & Vellekoop, I.M., 2016. A convergent Born series for solving the inhomogeneous Helmholtz equation in arbitrarily large media, *Journal of Computational Physics*, **322**, 113–124.

Pelissetto, A. & Vicari, E., 2002. Critical phenomena and renormalization-group theory, *Physics Reports*, **368**, 549–727.

Snieder, R., 1990. A perturbative analysis of non-linear inversion, *Geophysical Journal International*, **101**, 545–556.

Weglein, A.B., Araujo, F., Carvalho, P.M., Stiolt, R.H., Matson, K.K., Coates, R.T., Corrigan, D., Joster, D.J., Shaw, S.T. & Zhang, H., 2003. Inverse scattering series and seismic exploration, *Inverse problems*, **19**, R27–R83.

Weglein, A.B., Gasparotto, F.A., Carvalho, P.M. & Stolt, R.H., 1997. An inverse-scattering series method for attenuating multiples in seismic reflection data, *Geophysics*, **62**, 1975–1989.

Wilson, K.G., 1971. Renormalization group and critical phenomena. I. Renormalization group and the Kadanoff scaling picture, *Physical Review B*, **4**, 3174–3183.

Wu, R.S. & Huang, L., 1995. Reflected wave modeling in heterogeneous acoustic media using the De Wolf approximation, *Mathematical Methods in Geophysical Imaging III, International Society for Optics and Photonics*, **2571**, 176–187.

Wu, R.S., Luo, J. & Chen, G., 2016. Seismic envelope inversion and renormalization group theory: Nonlinear scale separation and slow dynamics, *SEG Technical Program Expanded Abstracts 2016*, **1**, 1346–1351.

Wu, R.S. & Toksoz, M.N., 1987. Difraction tomography and multisource holography applied to seismic imaging, *Geophysics*, **52**, 11–25.

Wu, R.S., Wang, B. & Hu, C., 2015. Renormalized nonlinear sensitivity kernel and inverse thin-slab propagator in T-matrix formalism for wave-equation tomography, *Inverse Problems*, **31**, 1–21.

Wu, R.S., Xie, X.B. & Wu, X.Y., 2007. One-way and one return approximations (De Wolf approximation) for fast elastic wave modeling in complex media, *Advances in Geophysics*, **48**, 265–322.

Wu, R.S. & Zheng, Y., 2014. Non-linear partial derivative and its De Wolf approximation for non-linear seismic inversion, *Geophysical Journal International*, **196**, 1827–1843.

Wu, Z. & Alkhalifah, T., 2017. Efficient scattering-angle enrichment for a nonlinear inversion of the background and perturbations components of a velocity model, *Geophysical Journal International*, **210**, 1981–1992.

Yakhot, V. & Orszag, S.A., 1986. Renormalization group analysis of turbulence. I. Basic theory, *Journal of Scientific Computing*, **1**, 3–51.

Yao, J., Lesage, A.C., Hussain, F. & Kouri, D.J., 2015. Scattering theory and Volterra renormalization for wave modeling in heterogeneous acoustic media, *SEG Technical Program Expanded Abstracts 2015*, **1**, 3594–3600.

Zhang, H. & Weglein, A.B., 2009. Direct nonlinear inversion of 1D acoustic media using inverse scattering subseries, *Geophysics*, **74**, WCD29–WCD39.

Zhdanov, M.S., 2002. *Geophysical Inverse Theory and Regularization Problems*, Elsevier.

Zuberi, M. & Alkhalifah, T., 2014. Generalized internal multiple imaging (GIMI) using Feynman-like diagrams, *Geophysical Journal International*, **197**, 1582–1592.